SUPPLEMENTARY INFORMATION

Polymersomes decorated with SARS-CoV-2 spike protein receptor binding domain elicit robust humoral and cellular immunity

Lisa R. Volpatti[1*], Rachel P. Wallace[1*], Shijie Cao[1*], Michal M. Raczy[1*], Ruyi Wang[1*], Laura T. Gray[1], Aaron T. Alpar[1], Priscilla S. Briquez[1], Nikolaos Mitrousis[1], Tiffany M. Marchell[2], Maria Stella Sasso[1], Mindy Nguyen[1], Aslan Mansurov[1], Erica Budina[1], Ani Solanki[3], Elyse A. Watkins[1], Mathew R. Schnorenberg[1], Andrew C. Tremain[2], Joseph W. Reda[1], Vlad Nicolaescu[4], Kevin Furlong[4], Steve Dvorkin[4], Shann S. Yu[1], Balaji Manicassamy[5], James L. LaBelle[6], Matthew V. Tirrell[1,7], Glenn Randall,[4] Marcin Kwissa[1], Melody A. Swartz[1,2,8,9+], Jeffrey A. Hubbell[1,2,9+]

[*]These authors contributed equally to this work

[1]Pritzker School of Molecular Engineering, University of Chicago, Chicago, IL 60637, United States

[2]Committee on Immunology, University of Chicago, Chicago, IL 60637, United States

[3]Animal Resources Center, University of Chicago, Chicago, IL 60637, United States

[4]Department of Microbiology, Howard T. Ricketts Laboratory, University of Chicago, Chicago, IL 60637, United States

[5]Department of Microbiology and Immunology, University of Iowa, Iowa City, IA 52242, United States

[6]Department of Pediatrics, University of Chicago Comer Children's Hospital, Chicago, IL 60637, United States

[7]Materials Science Division, Argonne National Laboratory, Lemont, IL 60439, United States

[8]Ben May Department of Cancer Research, University of Chicago, Chicago, IL 60637, United States

[9]Committee on Cancer Biology, University of Chicago, Chicago, IL 60637, United States

[+]Correspondence to melodyswartz@uchicago.edu, jhubbell@uchicago.edu

Table of Contents

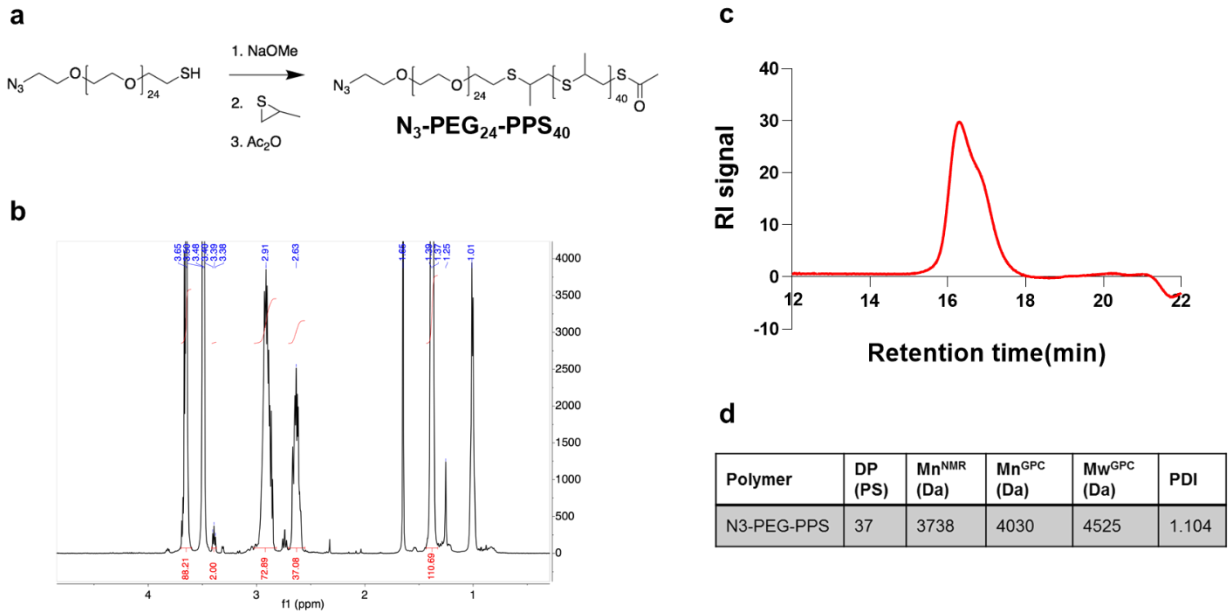

d

Polymer	DP (PS)	Mn^{NMR} (Da)	Mn^{GPC} (Da)	Mw^{GPC} (Da)	PDI
N3-PEG-PPS	37	3738	4030	4525	1.104

Supplementary Figure S1 | Synthesis and characterization of N_3-PEG-PPS. a, Synthetic route, **b,** ^{1}H NMR spectrum, **c,** gel permeation chromatography (GPC) trace, and **d,** summary of physiochemical properties of N_3-PEG-PPS.

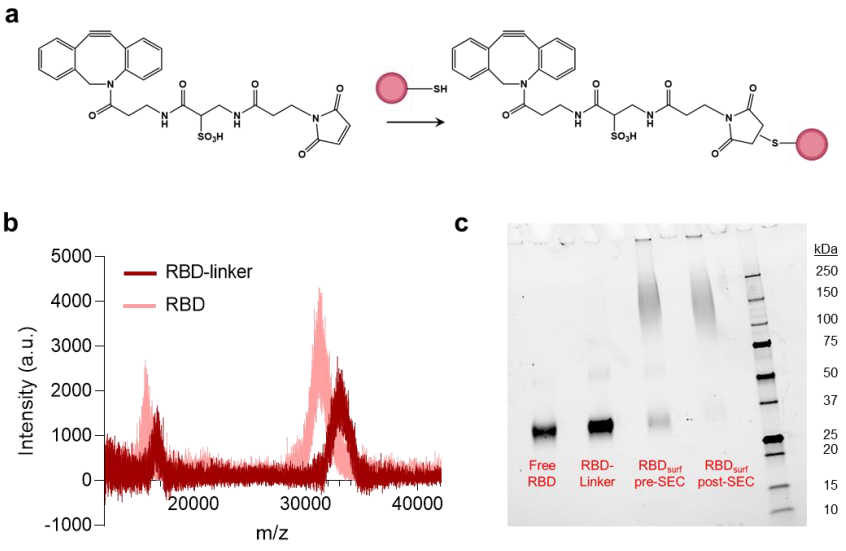

Supplementary Figure S2 | Synthesis and characterization of RBD-linker. a, Synthetic route, **b,** MALDI of RBD-linker and free RBD, **c,** SDS PAGE of free RBD, RBD-linker, RBD_{surf} before size exclusion chromatography (SEC) and purified RBD_{surf} post-SEC.

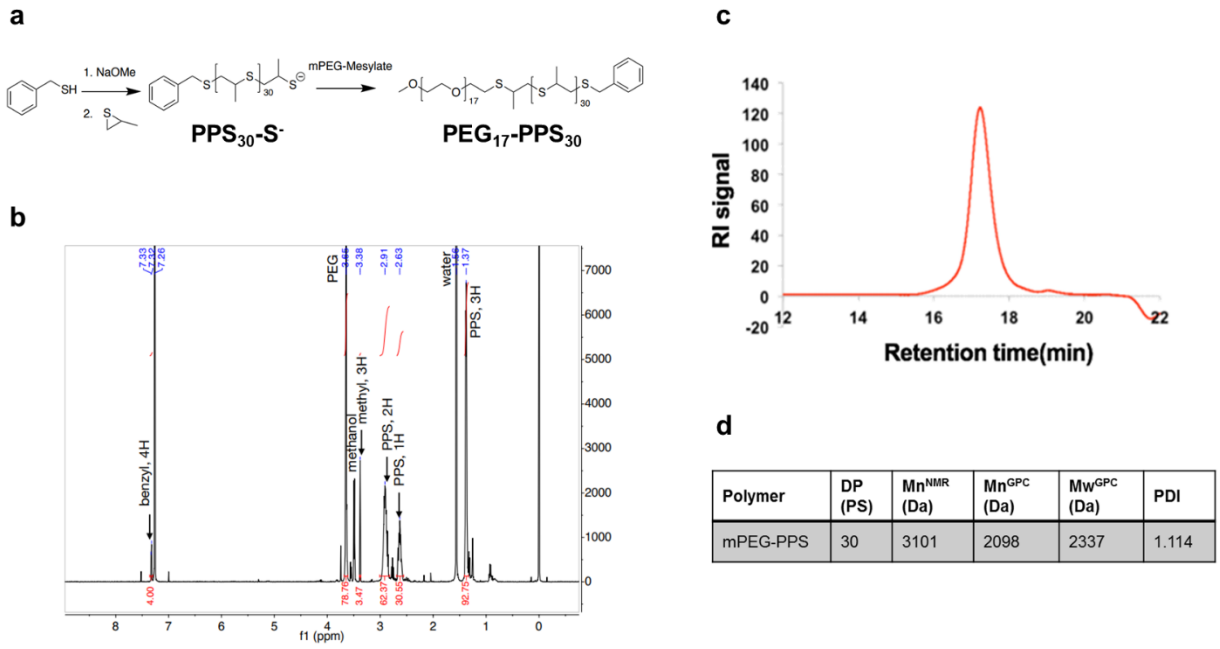

Polymer	DP (PS)	Mn^{NMR} (Da)	Mn^{GPC} (Da)	Mw^{GPC} (Da)	PDI
mPEG-PPS	30	3101	2098	2337	1.114

Supplementary Figure S3 | Synthesis and characterization of PEG-PPS. a, Synthetic route, **b,** ^{1}H NMR spectrum, **c,** gel permeation chromatography (GPC) trace, and **d,** summary of physiochemical properties of PEG-PPS.

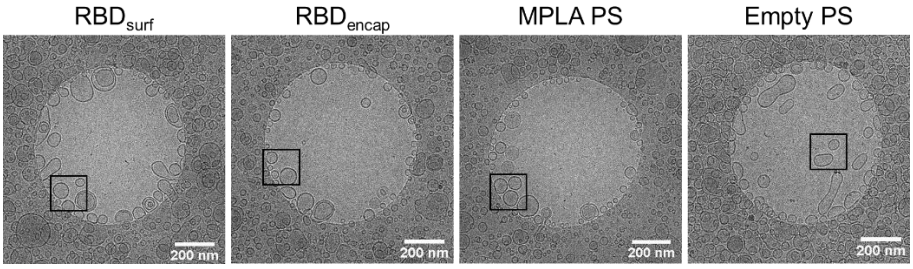

Supplementary Figure S4 | Additional cryoEM images of PS. Black box indicates magnified region in Figure 1b.

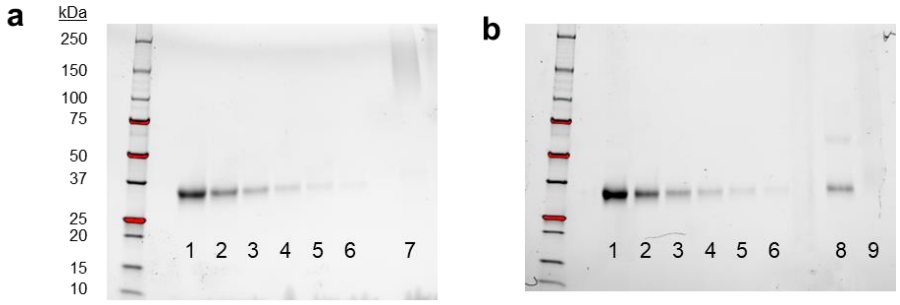

Supplementary Figure S5 | PS stability by SDS PAGE after > 180 d at 4 °C. SDS PAGE of **a,** RBD_{surf} and **b,** RBD_{encap}. Lanes 1-6 represent RBD standard curve values of 400, 200, 100, 50, 25, and 12.5 µg/mL. Lane 7 contains of RBD_{surf} disrupted with Triton X. Lane 8 contains of RBD_{encap} disrupted with Triton X, and Lane 9 contains undisrupted RBD_{encap}.

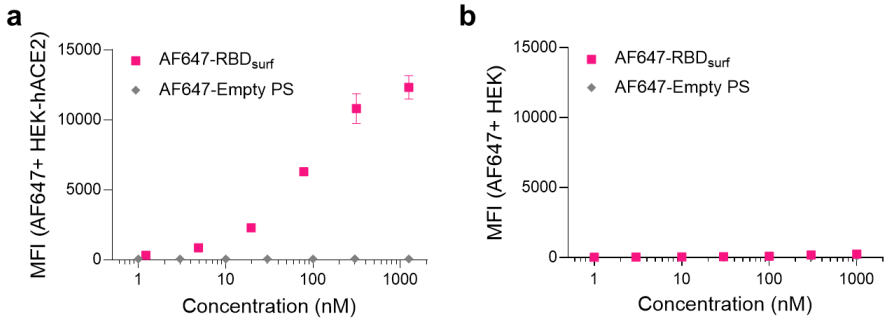

Supplementary Figure S6 | RBD binding to HEK-hACE2 and HEK-293 cells. a, Mean fluorescence intensity (MFI) of AF647-labeled RBD_{surf} and empty PS bound to HEK-hACE2 cells characterized by flow cytometry. **b,** MFI of AF647-labeled RBD_{surf} and empty PS indicating an absence of binding to control HEK-293 (HEK) cells. Data plotted as mean ± SD for n = 2 replicates.

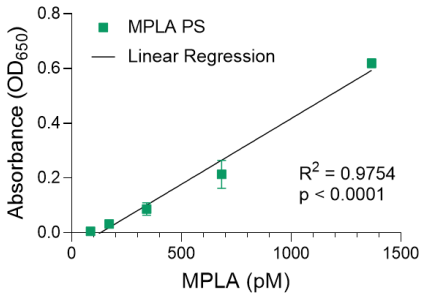

Supplementary Figure S7 | MPLA PS as a TLR4 agonist. Linear concentration-dependent stimulation of HEK-Blue™ TLR4 reporter cells with MPLA PS. Data plotted as mean ± SD for n = 3 replicates.

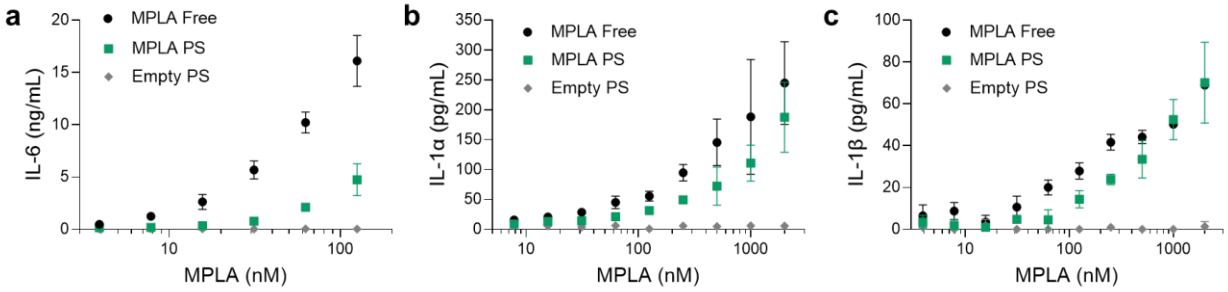

Supplementary Figure S8 | *In vitro* activity of MPLA PS. Dose-dependent secretion of **a,** IL-6, **b,** IL-1α, and **c,** IL-1β from cultured murine bone marrow-derived dendritic cells stimulated by free MPLA, MPLA PS, or empty PS. Data plotted as mean ± SD for n = 3 replicates.

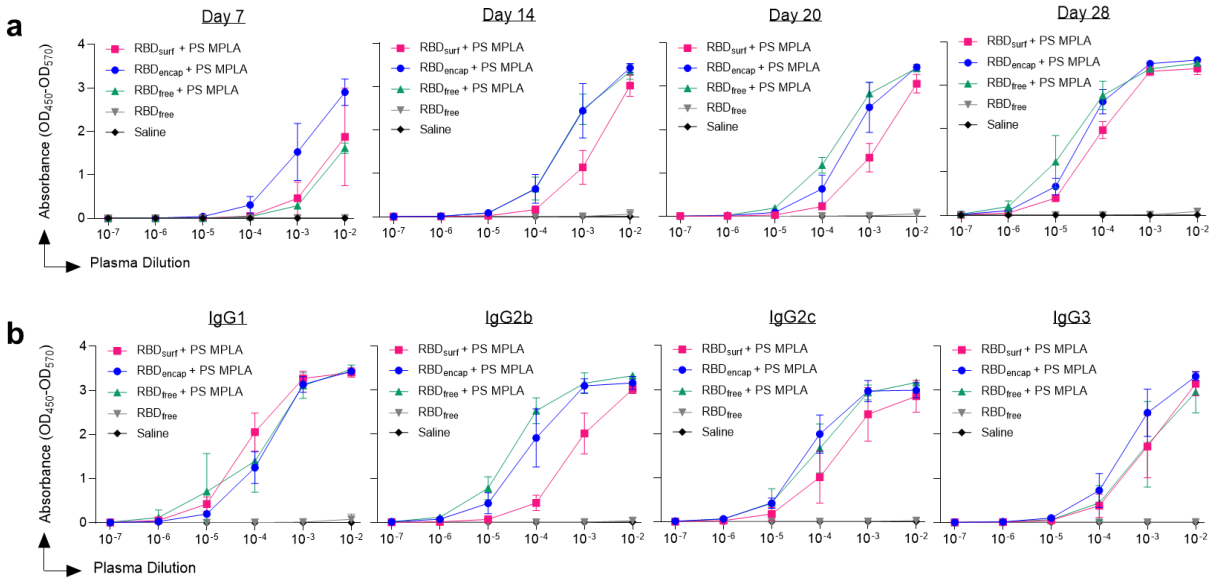

Supplementary Figure S9 | ELISA absorbance vs. dilution curves. Absorbance vs. dilution for RBD-specific ELISAs for **a,** total IgG over time and **b,** IgG subtypes on d28. Log-transformed curves were quantified by AUC in Figure 2. Data plotted as mean ± SD and represent 1 of 2 experiments with n = 5 mice each.

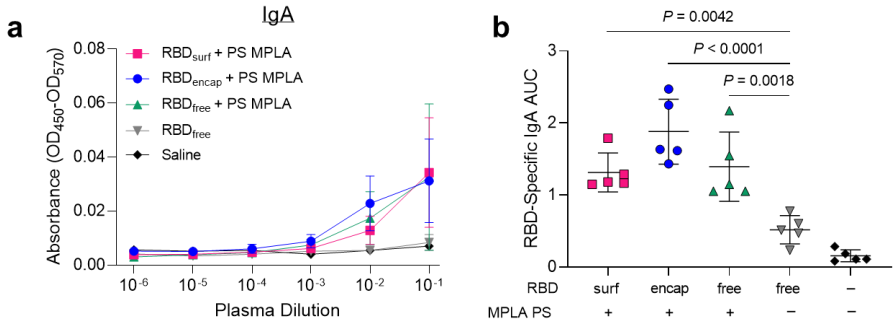

Supplementary Figure S10 | Presence of IgA antibodies. a, Absorbance vs. dilution for RBD-specific IgA ELISAs. **b,** AUC from (a). Data plotted as mean ± SD and represent 1 of 2 experiments with n = 5 mice each. Symbols in (b) represent individual mice. Comparisons to unadjuvanted RBD_{free} were made using one-way ANOVA with Dunn's post-test.

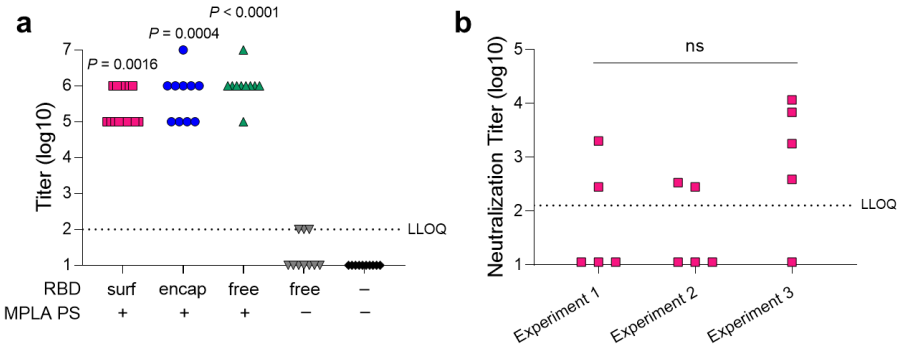

Supplementary Figure S11 | IgG antibody and viral neutralization titers. a, Aggregate RBD-specific IgG antibody titers 1 week post-boost based on ELISA. Values below the LLOQ (= 2) are plotted as LLOQ/2. Titers were determined as the -log of the lowest plasma dilution for which (OD450-OD570) – (average of blanks + 4 × standard deviation of blanks) > 0.01. *P* values represent comparisons to unadjuvanted RBD_{free}. **b)** Viral neutralization titers for RBD_{surf} + MPLA PS across three different cohorts of n = 5 mice, indicating experiment reproducibility. Values below the LLOQ (= 2.11) are plotted as LLOQ/2.; ns p = 0.11. Symbols represent individual mice. Comparisons were made using a Kruskal-Wallis nonparametric test with Dunn's post-test.

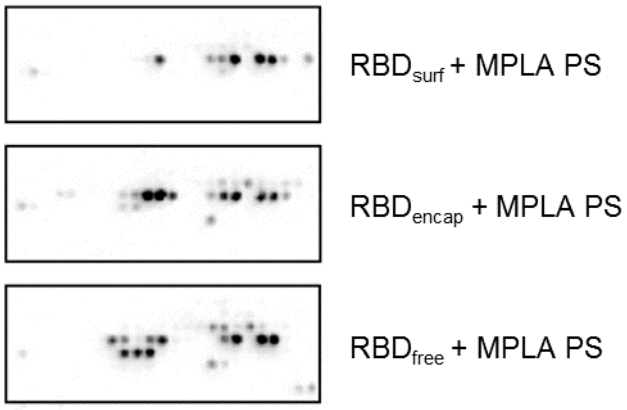

Supplementary Figure S12 | Representative peptide array images. Boxes represent region of peptide array specific to the RBD of the Spike protein. Peptide arrays quantified in Figure 3c.

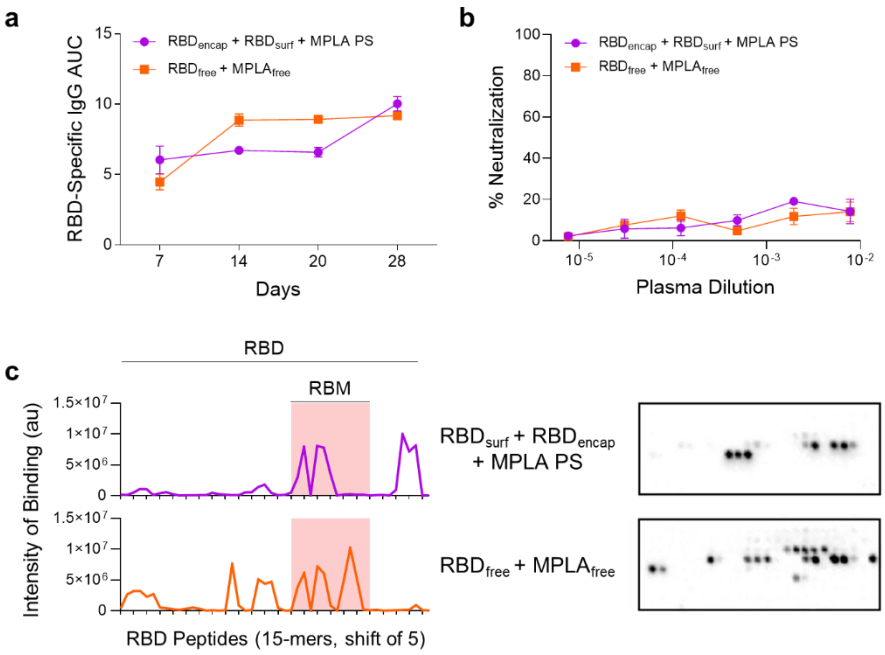

Supplementary Figure S13 | Analysis of plasma by mice vaccinated with RBD$_{surf}$ + RBD$_{encap}$ + MPLA PS and RBD$_{free}$ + MPLA$_{free}$. Mice received a priming dose on day 0 with a boost on day 21, and plasma was taken weekly to monitor production of RBD-specific antibodies. **a,** AUC of absorbance curve of RBD-specific IgG ELISAs for mice vaccinated with either 5 μg RBD$_{encap}$ + 5 μg RBD$_{surf}$ + MPLA PS or 10 μg RBD$_{free}$ + MPLA$_{free}$. Data plotted as mean ± SD for n = 5 mice. **b,** Neutralization of SARS-CoV-2 infection of Vero E6 cells *in vitro*. Data plotted as mean ± SEM for n = 5 mice. **c,** Epitope mapping using 15-amino-acid peptides with a 5-amino-acid shift, spanning the entire RBD sequence with representative images of peptide arrays.

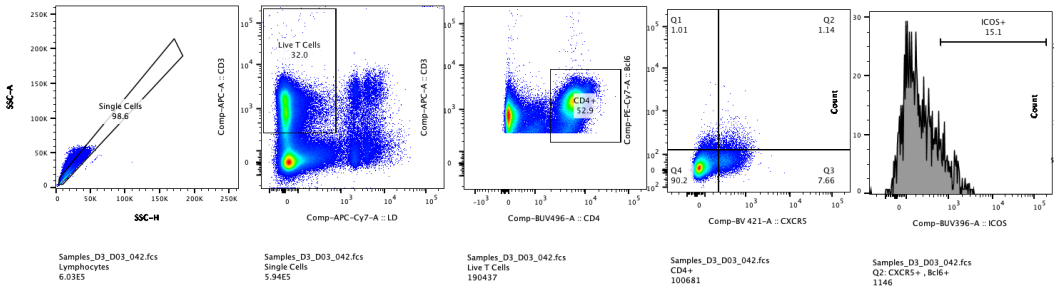

Supplementary Figure S14 | Representative T follicular helper cell gating strategy.

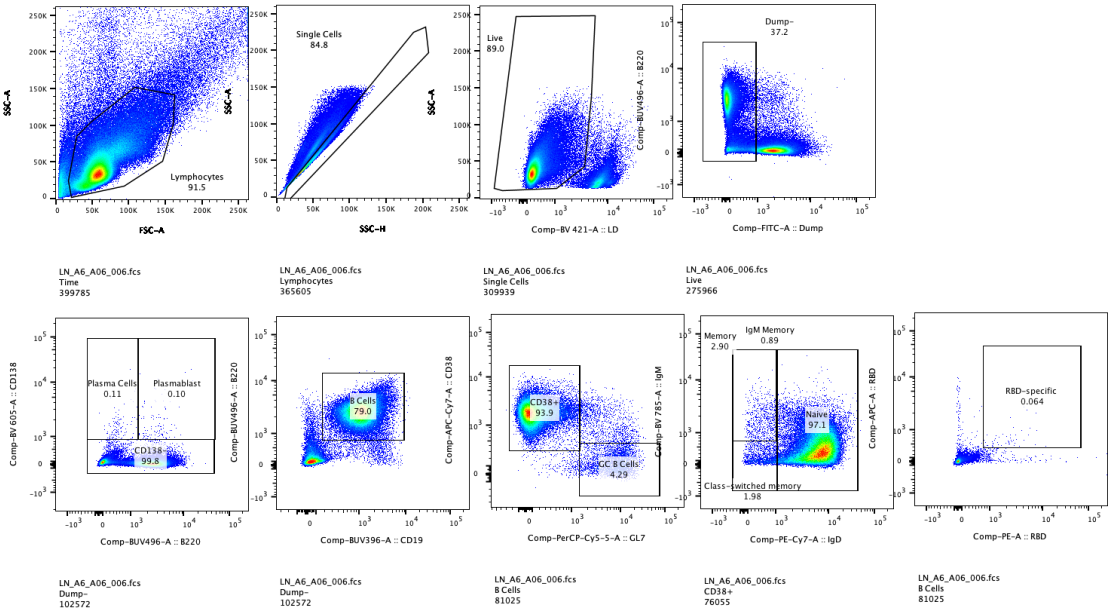

Supplementary Figure S15 | Representative B cell gating strategy.

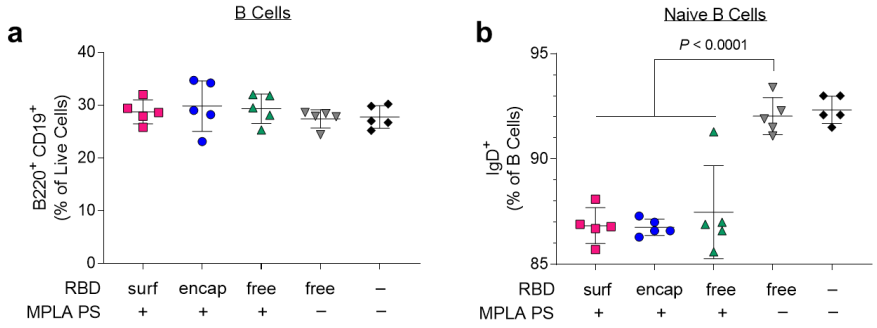

Supplementary Figure S16 | Total and naïve B cells in vaccinated mice 1 week post-boost. **a,** Total B cells ($B220^+$ $CD19^+$) and **b,** naïve B cells in dLNs. Data plotted as mean ± SD and represent 1 of 2 experiments with n = 5 mice each. Symbols represent individual mice. Comparisons to unadjuvanted RBD_{free} were made using one-way ANOVA with Dunn's post-test.

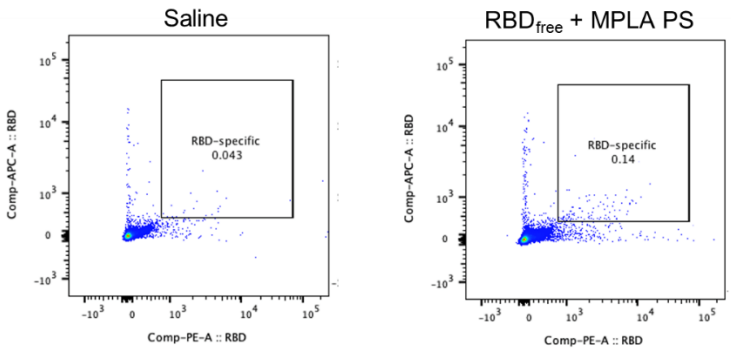

Supplementary Figure S17 | Representative tetramer staining.

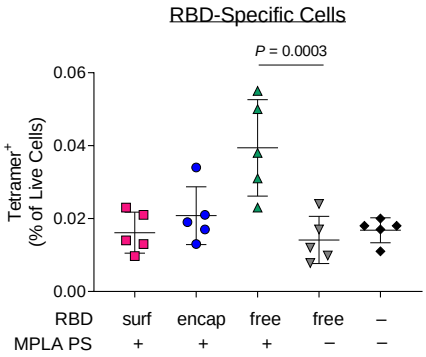

Supplementary Figure S18 | RBD-specific cells in vaccinated mice 1 week post-boost. Tetramer$^+$ cells in dLNs on d28. Data plotted as mean ± SD and represent 1 of 2 experiments with n = 5 mice each. Symbols represent individual mice. Comparisons to unadjuvanted RBD_{free} were made using one-way ANOVA with Dunn's post-test.

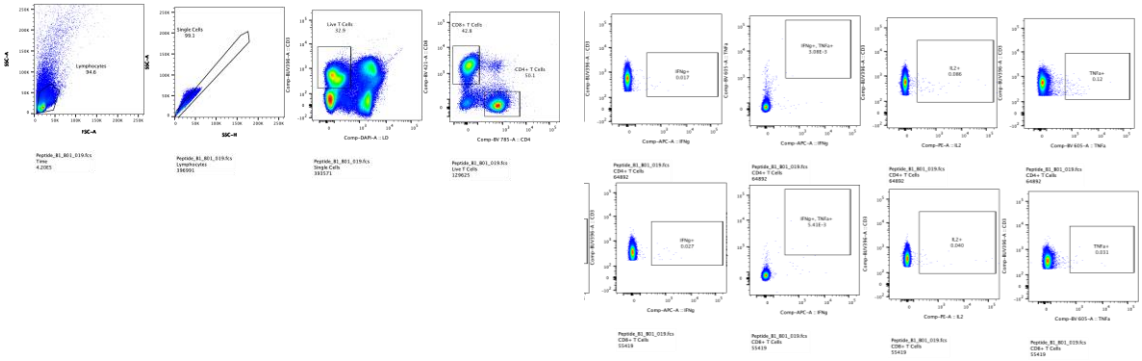

Supplementary Figure S19 | Representative intracellular cytokine gating strategy.

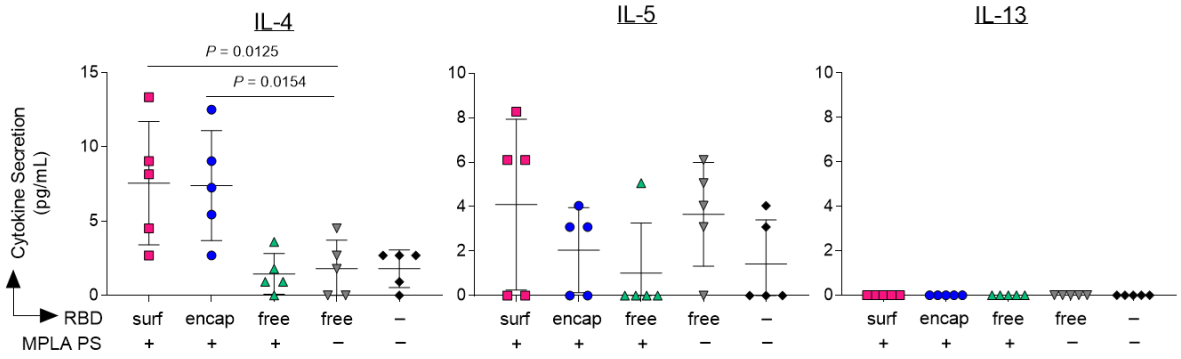

Supplementary Figure S20 | Th2-type cytokines secreted upon *ex vivo* stimulation with RBD. Lymph node cells isolated from the dLNs of PS vaccinated mice 1 week post-boost were restimulated *ex vivo* with full RBD protein. After 3 d, levels of IL-4, IL-5, and IL-13 secreted into the supernatant were measured. Data plotted as mean ± SD and represent 1 of 2 experiments with n = 5 mice each. Symbols represent individual mice. Comparisons to unadjuvanted RBD_{free} were made using one-way ANOVA with Dunn's post-test.

Supplementary Table S1 | Summary of loading capacities of PS.

	Polymer (mg mL^{-1})	Cargo (mg mL^{-1})	Loading (wt%)
RBD_{surf}	7.96	0.127	1.57
RBD_{encap}	7.00	0.125	1.75
MPLA PS	3.49	0.241	6.46

Polymer concentration was determined by GPC, RBD concentration in RBD_{surf} was determined by CBQCA protein quantitation assay, RBD concentration in RBD_{encap} was determined by SDS PAGE, and MPLA concentration was determined by mass spectrometry.

Supplementary Table S2 | Probes and antibodies for T_{fh} cell panel.

Marker	Color	Vendor
Viability Dye	eFluor 780	Invitrogen 65-0865-14
CD4	BV496	BD Horizon 612952
CD3	BUV737	BD Optibuild 741788
CD44	PerCpCy5.5	Invitrogen 45-0441-82
CXCR5	BV421	Biolegend 145512
ICOS	BUV396	BD Horizon 565885
Bcl6	PE-Cy7	Biolegend 358512

Supplementary Table S3 | Probes and antibodies for RBD-specific B cell panel.

Marker	Color	Vendor
Viability Dye	Violet fluorescent reactive dye	Invitrogen L34964A
RBD-tetramer	PE	-
RBD-tetramer	APC	-
F4/80 (Dump)	FITC	Biolegend 123107
CD11c (Dump)	FITC	Biolegend 117306
Ly6c(Dump)	FITC	Invitrogen 53-5932-82
Ly6g (Dump)	FITC	Invitrogen 11-9668-82
CD4 (Dump)	FITC	Biolegend 100406
CD8a (Dump)	FITC	Biolegend 100706
B220	BUV496	BD Horizon 612950
CD19	BUV396	BD Horizon 565965
CD138	BV605	Biolegend 142531
IgM	BV786	BD Optibuild 743328
IgD	PE-Cy7	Biolegend 405720
CD38	APC-Cy7	Biolegend 102727
GL7	PerCP-Cy5.5	Invitrogen 46-5902-82

Supplementary Table S4 | Probes and antibodies for restimulation panel.

Marker	Color	Vendor
Viability Dye	eFluor 455 (UV)	Invitrogen 65-0868-14
CD3	BUV395	BD Horizon 563565
CD4	BV786	BD Horizon 563331
CD8	BV421	BD Horizon 563898
IFNλ	APC	Biolegend 505810
TNFα	BV605	Biolegend 506329
IL-2	PE	BD Pharmigen 554428

Chemical Synthesis and Characterization

N_3-PEG-PPS. N_3-PEG-PPS was synthesized by first dissolving N_3-PEG_{24}-SH (1 eq, MW ~1000 g mol^{-1}; Nanosoft Polymers) in degassed, anhydrous THF and deprotonating the thiol group by addition of sodium methoxide (NaOMe; 1.1 eq) under nitrogen gas. Propylene sulfide (40 eq) was added by syringe, and the reaction proceeded until completion at the desirable degree of polymerization of PPS, as determined by ^{1}H NMR. The polymer was precipitated multiple times in ice cold methanol to obtain the final product, N_3-PEG_{24}-PPS_{40}, characterized by ^{1}H NMR (400 MHz Bruker DRX spectrometer equipped with a BBO probe, using Topspin 1.3) and gel permeation chromatography (GPC; Tosoh EcoSEC size exclusion chromatography system with a Tosoh SuperAW3000 column). ^{1}H-NMR (400 MHz, $CDCl_3$) of N_3-PEG-PPS, δ 1.37 (s, PPS, 3H), 2.63 (m, PPS, 1H), 2.91 (m, PPS, 2H), 3.39 (t, -CH_2-N_3, 2H), 3.65 (m, PEG).

PEG-PPS. PEG-PPS was synthesized as previously described[1]. Briefly, benzyl mercaptan (1 eq.) in degassed, anhydrous THF (20 mM) was deprotonated with NaOMe (1.1 eq.). Under nitrogen protection, propylene sulfide (39 eq) was rapidly added by syringe, and the reaction proceeded until completion at the desirable degree of polymerization of PPS, as determined by ^{1}H NMR. Subsequently, $mPEG_{17}$-mesylate (synthesized in-house as previously described[1]) was added, and the mixture was allowed to react overnight. The polymer was precipitated multiple times in ice cold methanol to obtain the final product, PEG_{17}-PPS_{30}, characterized by ^{1}H NMR and GPC. ^{1}H-NMR (400 MHz, $CDCl_3$) of mPEG-PPS, δ 1.37 (s, PPS, 3H), 2.63 (m, PPS, 1H), 2.91 (m, PPS, 2H), 3.38 (m, -OCH_3, 3H), 3.65 (m, PEG), 7.32 (m, benzyl, 4H).

[1]Scott, E. A. *et al.* Dendritic cell activation and T cell priming with adjuvant- and antigen-loaded oxidation-sensitive polymersomes. *Biomaterials* **33**, 6211–6219 (2012).